Vector Control Strategies to Enable Equal Frequency Operation of the Modular Multilevel Matrix Converter

***M. Diaz*[1], *M. Espinosa*[2], *F. Rojas*[1], *P. Wheeler*[3], *R. Cardenas*[4]**

[1]*University of Santiago of Chile, Chile, matias.diazd@usach.cl, felix.rojas@usach.cl*

[2]*University of Costa Rica, Costa Rica, maeb@ieee.org,* [3]*The University of Nottingham, United Kingdom, pat.wheeler@nottingham.ac.uk,* [4]*University of Chile, rcd@ieee.org*

***Abstract*—The Modular Multilevel Matrix Converter (M^3C) is an ac-to-ac converter suitable for high-power applications. The control of this converter is complex, mainly when the frequencies of the ac systems connected to the ports of the converter are close or equal, because the floating capacitors can present large voltage oscillations. Therefore, this paper proposes a new Vector Control System to enable the operation of the M^3C when the input-output frequencies are equal. The effectiveness of the proposal is validated through simulations and experimental results conducted with a 27 power-cell prototype.**

***Index Terms*—Modular Multilevel Matrix Converter, Equal Frequencies Operation, Floating Capacitor Voltage Control**

I. Introduction

The M^3C is an ac-to-ac converter firstly proposed for Wind Energy Conversion Systems [1]. This converter has several advantages over traditional topologies such as full modularity, simple extension to reach high voltage levels, redundancy, control flexibility and power quality [2]. Lately, the M^3C has been also proposed for drives [3], [4], large power wind turbines [5], [6] and grid-connected applications [7].

The M^3C is characterised by a cascade connection of Full-Bridge power cells forming a cluster. The direct ac-to-ac connection of two ac ports is achieved using the nine cluster of the converter, as shown in Fig. 1. The capacitor voltage of each power cell is floating and can charge-discharge during the operation of the converter. Therefore, one of the most important control tasks is to maintain the voltage in each capacitor within an acceptable range [2].

This converter is suitable for low-speed high-power applications because lower circulating currents and common-mode voltage are required to mitigate the oscillations in the capacitors, in comparison to other topologies such as the Modular Multilevel Converter [2]. However, the M^3C has an inherent problem when the input-port frequency is close to the output-port frequency, resulting in large voltage oscillations in the floating capacitors.

Cascade control systems based on decoupled modelling of the M^3C have been proposed [3], [4]. These approaches enable the use of the circulating current of the converter and the common-mode voltage to regulate the floating capacitor voltages. When the input-port frequency is low in comparison to the output-port frequency, referred to as Low-Frequency Mode (LFM), the average components of the capacitor voltages are controlled using either the circulating currents or the common-mode voltages [3]–[6], [8]. When the input-port

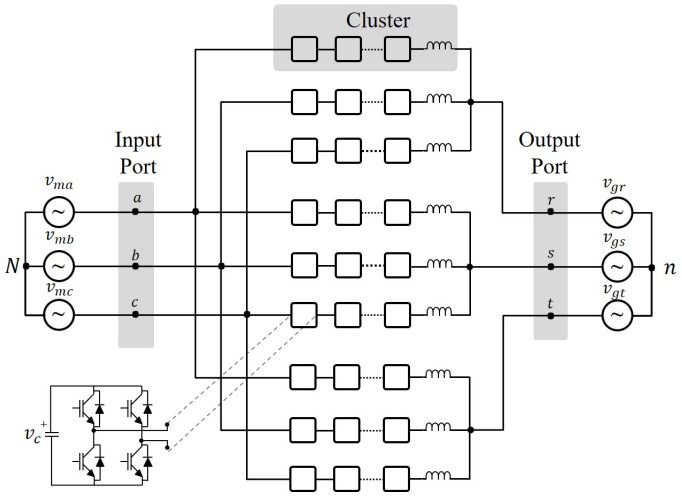

Fig. 1: Modular Multilevel Matrix Converter Topology.

frequency is close or similar to the output-port frequency, referred to as Equal Frequencies Mode (EFM), mitigation signals are included to compensate the oscillations in the floating capacitor voltages [7], [9]. These mitigation signals are predefined offline and, consequently, do not have closed-loop adaptation capability. Additionally, the mitigation currents signals cannot compensate nonlinearities or simplifications of the converter model, and they do not adequately regulate the voltage oscillations to zero.

To solve the problems above, this paper presents a novel dq Vector Control System to enable EFM operation of the M^3C. This proposal considers nested control systems to regulate the floating capacitor voltages and the input-output ports. In EFM, the mitigation signals are regulated using a closed-loop controller that successfully drives the oscillations in the floating capacitor voltages to zero. The effectiveness of the proposed Control Strategies is validated through experiments conducted with a 27 power cells prototype rated to 5kVA.

II. Modular Multilevel Matrix Converter

The dynamics of the M^3C can be represented by a decoupled model obtained using the Double $\alpha\beta 0$ Transformation [3], [4]. This procedure enables a decoupled representation of the Voltages-Currents and Power-Capacitor Voltages of the M^3C as follows:

A. Voltage-Current Model of the M^3C

The first model represents the currents and voltages of the M^3C in Double $\alpha\beta 0$ coordinates:

$$\sqrt{3}\begin{bmatrix} 0 & 0 & 0 \\ 0 & 0 & 0 \\ v_{m_\alpha} & v_{m_\beta} & 0 \end{bmatrix} = L_c \frac{d}{dt}\begin{bmatrix} i_{\alpha\alpha} & i_{\beta\alpha} & i_{0\alpha} \\ i_{\alpha\beta} & i_{\beta\beta} & i_{0\beta} \\ i_{\alpha 0} & i_{\beta 0} & i_{00} \end{bmatrix} + \begin{bmatrix} v_{\alpha\alpha} & v_{\beta\alpha} & v_{0\alpha} \\ v_{\alpha\beta} & v_{\beta\beta} & v_{0\beta} \\ v_{\alpha 0} & v_{\beta 0} & v_{00} \end{bmatrix} + \sqrt{3}\begin{bmatrix} 0 & 0 & v_{g_\alpha} \\ 0 & 0 & v_{g_\beta} \\ 0 & 0 & 0 \end{bmatrix} + \begin{bmatrix} 0 & 0 & 0 \\ 0 & 0 & 0 \\ 0 & 0 & 3v_n \end{bmatrix} \quad (1)$$

Where the m represents the input-port voltages and currents and the subscript g stands for the output-port variables. The voltages at the terminal of the cluster are represented by v_{xy}, $x \in \{\alpha, \beta\}$, $y \in \{\alpha, \beta\}$, L_c is the cluster inductor inductance, and the common-mode voltage between the neutral points N and n is symbolised by v_n.

One of the main advantages of (1) is the fact that it enables the use of the transformed cluster currents and voltages as degrees of freedom to regulate the converter. The currents $i_{\alpha 0}$ and $i_{\beta 0}$ are only dependent on the input-port currents, whereas $i_{0\alpha}$ and $i_{0\beta}$ are only dependent on the output-port currents. Furthermore, the currents $i_{\alpha 0}$, $i_{\beta 0}$, $i_{0\alpha}$ and $i_{0\beta}$ are known as Circulating Currents.

B. Power-Cap. Voltage Model of the M^3C

The total capacitor voltage available in a cluster, referred to as Cluster Capacitor Voltage (CCV), can be related to the cluster power as follows [6]:

$$Cv_c^* \frac{d}{dt}\begin{bmatrix} v_{c_{ar}} & v_{c_{as}} & v_{c_{at}} \\ v_{c_{br}} & v_{c_{bs}} & v_{c_{bt}} \\ v_{c_{cr}} & v_{c_{cs}} & v_{c_{ct}} \end{bmatrix} \approx \begin{bmatrix} P_{ar} & P_{as} & P_{at} \\ P_{br} & P_{bs} & P_{bt} \\ P_{cr} & P_{cs} & P_{ct} \end{bmatrix} \quad (2)$$

Note that it is assumed that the power cells have the same capacitance C and their capacitors are controlled to the desired value v_c^*.

The Double $\alpha\beta 0$ Transformation is applied to (2) to enable a decoupled representation of the energy interaction among all the clusters of the M^3C [4]. Accordingly, (2) results in:

$$Cv_c^* \frac{d}{dt}\begin{bmatrix} v_{c_{\alpha\alpha}} & v_{c_{\beta\alpha}} & v_{c_{0\alpha}} \\ v_{c_{\alpha\beta}} & v_{c_{\beta\beta}} & v_{c_{0\beta}} \\ v_{c_{\alpha 0}} & v_{c_{\beta 0}} & v_{c_{00}} \end{bmatrix} \approx \begin{bmatrix} P_{\alpha\alpha} & P_{\beta\alpha} & P_{0\alpha} \\ P_{\alpha\beta} & P_{\beta\beta} & P_{0\beta} \\ P_{\alpha 0} & P_{\beta 0} & P_{00} \end{bmatrix} \quad (3)$$

The voltage terms of the left side of (3) represent voltage imbalances between different clusters. Additionally, $v_{c_{00}}$ is related to the total active power flowing into/from the M^3C. The power components in the right-side of (3) can be expressed as a function of the transformed currents and voltages of the converter as presented in [4]. For instance, $P_{\alpha\alpha}$ yields to:

$$P_{\alpha\alpha} = \frac{(v_{m\alpha} i_{g\alpha} - v_{g\alpha} i_{m\alpha})}{3} + \frac{(v_{m\alpha} i_{\alpha\alpha} - v_{m\beta} i_{\beta\alpha})}{\sqrt{6}} - \frac{(v_{g\alpha} i_{\alpha\alpha} - v_{g\beta} i_{\alpha}\ )}{\sqrt{6}} - v_n i_{\alpha\alpha} \quad (4)$$

Then, replacing (4) into (3):

$$\tilde{v}_{c_{\alpha\alpha}} \approx \frac{V_m I_g \sin(\phi_g + (\omega_g - \omega_m)t) + V_g I_m \sin(\phi_m - (\omega_g - \omega_m)t)}{6Cv_c^*(\omega_g - \omega_m)} + \frac{V_m I_g \sin(\phi_g + (\omega_g + \omega_m)t) - V_g I_m \sin(\phi_m + (\omega_g + \omega_m)t)}{6Cv_c^*(\omega_g + \omega_m)} \quad (5)$$

where $\omega_m = 2\pi f_m$ and $\omega_g = 2\pi f_g$. Note that V_m and V_g are the machine and output-port phase-to-neutral peak voltage magnitudes, respectively. I_m and I_g are the machine and output-port peak current magnitudes, respectively. f_m and f_g are the machine and output-port frequencies. The angles ϕ_m and ϕ_g are the machine and output-port phase angles.

Analysing (5), it is possible to conclude that the CCVs can present large voltage oscillations when $f_m = \pm f_g$. The same problem appears in $v_{c_{\alpha\beta}}$, $v_{c_{\beta\alpha}}$ and $v_{c_{\beta\beta}}$ when $f_m = \pm f_g$. Additionally, CCVs $v_{c_{\alpha 0}}$ and $v_{c_{\beta 0}}$ can lead to large voltage fluctuations when $f_m = 0$ and $v_{c_{0\alpha}}$ and $v_{c_{0\beta}}$ when $f_g = 0$.

C. $\Sigma\Delta$ Transformation

This proposal introduces the use of an additional linear transformation, called $\Sigma\Delta$ Transformation [10], [11], to enable a vector representation of the Power-CCV model. The $\Sigma\Delta$ Transformation can be written in matrix form to transform a generic vector $\vec{X}$ from the Double-$\alpha\beta 0$ frame to the $\Sigma\Delta$ frame as follow:

$$\begin{bmatrix} X_{1\alpha}^{\Sigma\Delta} \\ X_{1\beta}^{\Sigma\Delta} \\ X_{2\alpha}^{\Sigma\Delta} \\ X_{2\beta}^{\Sigma\Delta} \end{bmatrix} = \frac{1}{2}\begin{bmatrix} 1 & 0 & 0 & 1 \\ 0 & 1 & -1 & 0 \\ 1 & 0 & 0 & -1 \\ 0 & 1 & 1 & 0 \end{bmatrix}\begin{bmatrix} X_{\alpha\alpha} \\ X_{\alpha\beta} \\ X_{\beta\alpha} \\ X_{\beta\beta} \end{bmatrix} \quad (6)$$

The $\Sigma\Delta$ Transformation is applied to (3) yielding to the Power-CCV of the M^3C in $\Sigma\Delta$ Double-$\alpha\beta 0$ coordinates:

$$Cv_c^*\begin{bmatrix} v_{c_{1\alpha}}^{\Sigma\Delta} & v_{c_{1\beta}}^{\Sigma\Delta} & v_{c_{0\alpha}} \\ v_{c_{2\alpha}}^{\Sigma\Delta} & v_{c_{2\beta}}^{\Sigma\Delta} & v_{c_{0\beta}} \\ v_{c_{\alpha 0}} & v_{c_{\beta 0}} & v_{c_{00}} \end{bmatrix} \approx \begin{bmatrix} P_{1\alpha}^{\Sigma\Delta} & p_{1\beta}^{\Sigma\Delta} & P_{0\alpha} \\ P_{2\alpha}^{\Sigma\Delta} & p_{2\beta}^{\Sigma\Delta} & P_{0\beta} \\ P_{\alpha 0} & P_{\beta 0} & P_{00} \end{bmatrix} dt \quad (7)$$

The use of the $\Sigma\Delta$ Transformation enables a better representation of the CCVs in terms of the ports frequencies because a pair of of CCV ripple terms is obtained for each unstable condition. For example, large voltage oscillations can appear in $\vec{v}_{c_{1\alpha\beta}}^{\Sigma\Delta}$ just when $f_m = f_g$ (and not when $f_m = \pm f_g$ as $v_{c_{\alpha\alpha}}$). Defining the power flows and the cluster capacitor voltages as vectors, the Vector Power-CCV model in $\Sigma\Delta$ Double-$\alpha\beta 0$ coordinates can be expressed as follows:

$$Cv_c^* \frac{d\vec{v}_{c_{1\alpha\beta}}^{\Sigma\Delta}}{dt} \approx \frac{1}{6}(\vec{v}_{m_{\alpha\beta}}^{\ c}\vec{i}_{g_{\alpha\beta}} - \vec{v}_{g_{\alpha\beta}}\vec{i}_{m_{\alpha\beta}}^{\ c}) + \frac{1}{\sqrt{6}}(\vec{v}_{m_{\alpha\beta}}\vec{i}_{2\alpha\beta}^{\Sigma\Delta} - \vec{v}_{g_{\alpha\beta}}^{\ c}\vec{i}_{2\alpha\beta}^{\Sigma\Delta^c}) - v_n\vec{i}_{1\alpha\beta}^{\Sigma\Delta} \quad (8)$$

$$Cv_c^* \frac{d\vec{v}_{c_{2\alpha\beta}}^{\Sigma\Delta}}{dt} \approx \frac{1}{6}(\vec{v}_{m_{\alpha\beta}}\vec{i}_{g_{\alpha\beta}} - \vec{v}_{g_{\alpha\beta}}\vec{i}_{m_{\alpha\beta}}) + \frac{1}{\sqrt{6}}(\vec{v}_{m_{\alpha\beta}}^{\ c}\vec{i}_{1\alpha\beta}^{\Sigma\Delta} - \vec{v}_{g_{\alpha\beta}}^{\ c}\vec{i}_{1\alpha\beta}^{\Sigma\Delta^c}) - v_n\vec{i}_{2\alpha\beta}^{\Sigma\Delta} \quad (9)$$

$$Cv_c^* \frac{d\vec{v}_{c_0}^{\alpha\beta}}{dt} \approx \frac{1}{3\sqrt{2}}(\vec{v}_{m_{\alpha\beta}}^{\ c}\vec{i}_{m_{\alpha\beta}}^{\ c}) - \frac{1}{\sqrt{3}}(\vec{v}_{g_{\alpha\beta}}\vec{i}_{1\alpha\beta}^{\Sigma\Delta^c} + \vec{v}_{g_{\alpha\beta}}^{\ c}\vec{i}_{2\alpha\beta}^{\Sigma\Delta}) - \frac{1}{\sqrt{3}}v_n\vec{i}_{m_{\alpha\beta}} \quad (10)$$

$$Cv_c^*\frac{d\vec{v}_{c_{\alpha\beta}}^{\,0}}{dt}\approx\frac{-1}{3\sqrt{2}}(\vec{v}_{g_{\alpha\beta}}^{\,c}\vec{i}_{g_{\alpha\beta}}^{\,c}) + \frac{1}{\sqrt{3}}(\vec{v}_{m_{\alpha\beta}}\vec{i}_{1\alpha\beta}^{\Sigma\Delta}+\vec{v}_{m_{\alpha\beta}}^{\,c}\vec{i}_{2\alpha\beta}^{\Sigma\Delta}) - \frac{1}{\sqrt{3}}v_n\vec{i}_{g_{\alpha\beta}} \quad (11)$$

The superscript c represents the complex conjugate operator. (8)−(11) represent the vector Power-CCV model of the M^3C. This model allows a simple analysis and implementation of vector control structures.

III. Vector Control Systems of the M^3C

Significant voltage oscillation should be avoided in $\vec{v}_{c_{1\alpha\beta}}^{\,\Sigma\Delta}$, $\vec{v}_{c_{2\alpha\beta}}^{\,\Sigma\Delta}$,$\vec{v}_{c_0}^{\,\alpha\beta}$ and $\vec{v}_{c_{\alpha\beta}}^{\,0}$ when the input-output ports frequencies are close. Notice that, due to the integral effect produced in the capacitors, even small dc-components in the powers components of (3) could produce significant voltage imbalances. Consequently, zero steady-state error and good dynamic control of the cluster capacitor voltage unbalances are fundamental to provide proper operation of the converter. Therefore, this proposal considers novel Control Strategies for decoupled regulation of the CCVs, input-port and the output-port Control is proposed. Each Control System is described in the following subsections.

A. Vector Control System of the CCVs

Vector Control Strategies for the regulation of $\vec{v}_{c_{1\alpha\beta}}^{\,\Sigma\Delta}$, $\vec{v}_{c_{2\alpha\beta}}^{\,\Sigma\Delta}$,$\vec{v}_{c_0}^{\,\alpha\beta}$ and $\vec{v}_{c_{\alpha\beta}}^{\,0}$ are proposed. The average value of all the floating capacitor voltages is regulated using $v_{c_{00}}$. In EFM, the CCV vectors (average and oscillation components) are regulated to zero using the last terms of (8)-(11).

It is important to mention that the control of the M^3C in LFM is not included in this proposal. However, readers can refer to [4], [6] for more details about the operation of the M^3C in LFM.

1) Control of the average component of the capacitor voltages: The term $v_{c_{00}}$ represents the average voltage in all the floating capacitors of the M^3C and it is related to the active power flowing into the converter P_{00}. Therefore, the following expression is written:

$$Cv_c^*\frac{dv_{c_{00}}}{dt}\approx P_{00}=\frac{\overbrace{(v_{m\alpha}i_{m\alpha}+v_{m\beta}i_{m\beta})}^{\text{Input Power}=P_{in}}}{3}-\frac{\overbrace{(v_{g\alpha}i_{g\alpha}+v_{g\beta}i_{g\beta})}^{\text{Output Power}=P_{out}}}{3} \quad (12)$$

The term P_{out} represents the M^3C output power which is considered as a disturbance that can be feed-forwarded for control purposes. Additionally, the input-port variables can be referred to a dq frame rotating at θ_m and oriented along the voltage vector. Therefore, (12) becomes:

$$Cv_c^*\frac{dv_{c_{00}}}{dt}\approx P_{00}=\frac{1}{3}v_{md}i_{md} \quad (13)$$

Accordingly, an incremental current $i_{md_1}^*$ can be calculated to regulate the average value of the CCVs using 13.

2) Control of $\vec{v}_{c_{1\alpha\beta}}^{\,\Sigma\Delta}$ and $\vec{v}_{c_{2\alpha\beta}}^{\,\Sigma\Delta}$: The power flows produced by the last terms of (8)-(9) are used to regulate the vectors $\vec{v}_{c_{1\alpha\beta}}^{\Sigma\Delta}$ and $\vec{v}_{c_{2\alpha\beta}}^{\Sigma\Delta}$ when the frequencies are close to $f_m=\pm f_g$.

The proposed control system is analysed in dq coordinates. Therefore, (8) is referred to a dq-frame using $\theta_{u1}=\int(\omega_g-\omega_m)dt$, and (9) is referred to a dq-frame rotating using $\theta_{u2}=\int(\omega_g+\omega_m)dt$:

$$Cv_c^*[\frac{d\vec{v}_{c_{1dq}}^{\Sigma\Delta}}{dt}+j\omega_{u1}\vec{v}_{c_{1dq}}^{\Sigma\Delta}]\approx\frac{1}{6}(\vec{v}_{m_{dq}}\vec{i}_{g_{dq}}-\vec{v}_{g_{dq}}\vec{i}_{m_{dq}}) + \frac{1}{\sqrt{6}}(\vec{v}_{m_{dq}}\vec{i}_{2_{dq}}^{\Sigma\Delta}e^{j3\theta_m}-\vec{v}_{g_{dq}}\vec{i}_{2_{dq}}^{\Sigma\Delta}e^{-j3\theta_g})-v_n(\vec{i}_{1_{dq}}^{\Sigma\Delta}) \quad (14)$$

$$Cv_c^*[\frac{d\vec{v}_{c_{2dq}}^{\Sigma\Delta}}{dt}+j\omega_{u2}\vec{v}_{c_{2dq}}^{\Sigma\Delta}]\approx\frac{1}{6}(\vec{v}_{m_{dq}}\vec{i}_{g_{dq}}-\vec{v}_{g_{dq}}\vec{i}_{m_{dq}}) + \frac{1}{\sqrt{6}}(\vec{v}_{m_{dq}}\vec{i}_{1_{dq}}^{\Sigma\Delta}e^{-j3\theta_m}-\vec{v}_{g_{dq}}\vec{i}_{1_{dq}}^{\Sigma\Delta}e^{-j3\theta_g})-v_n(\vec{i}_{2_{dq}}^{\Sigma\Delta}) \quad (15)$$

The common-mode voltage and the dq circulating currents should be in phase to produce adjustable power flows. Additionally, $\vec{i}_{1_{dq}}^{\Sigma\Delta}$ and $\vec{i}_{2_{dq}}^{\Sigma\Delta}$ are redefined as high frequency signals and then the power flows produced by middle terms of (8)-(9) can be neglected since the capacitors filter them out. Therefore, the dq circulating currents and the common-mode voltage are defined as:

$$\vec{i}_{1dq_3}^{\Sigma\Delta*}=\vec{I}_{1dq_3}^{\Sigma\Delta*}f(t);\vec{i}_{2dq_3}^{\Sigma\Delta*}=\vec{I}_{2dq_3}^{\Sigma\Delta*}f(t);v_n=V_0g(t) \quad (16)$$

where $f(t)$ and $g(t)$ are in phase. What is more, $f(t)=A_1\sin\theta_n+A_3\sin 3\theta_n$, where θ_n must be relatively high frequency signal, and $g(t)=sign\{f(t)\}$. The amplitudes of the constants A_1, A_3 and V_0 are chosen accordingly to the criteria presented in [12]. These definitions imply than the mean value of $f(t)g(t)\approx 1$. Then, (14)-(15) yields to:

$$Cv_c^*\frac{d\vec{v}_{c_{1dq}}^{\,\Sigma\Delta}}{dt}\approx\frac{1}{6}(\vec{v}_{m_{dq}}\vec{i}_{g_{dq}}-\vec{v}_{g_{dq}}\vec{i}_{m_{dq}})-V_0\vec{I}_{1dq_3}^{\,\Sigma\Delta} \quad (17)$$

$$Cv_c^*\frac{d\vec{v}_{c_{2dq}}^{\,\Sigma\Delta}}{dt}\approx\frac{1}{6}(\vec{v}_{m_{dq}}\vec{i}_{g_{dq}}-\vec{v}_{g_{dq}}\vec{i}_{m_{dq}})-V_0\vec{I}_{2dq_3}^{\,\Sigma\Delta} \quad (18)$$

The voltage oscillations in (17)−(18) can be considered as disturbances from a control point of view. This interpretation leads to the redefinition of the dq circulating considering the next feed-forward components:

$$\vec{I}_{1_{dq}}^{\Sigma\Delta}=\vec{I}_{1_{dqc}}^{\Sigma\Delta}+\vec{I}_{1_{dq}f}^{\,\Sigma\Delta};\ \vec{I}_{1_{dq}f}^{\,\Sigma\Delta}=\frac{(\vec{v}m_{dq}\vec{i}_{g_{dq}}-\vec{v}_{g_{dq}}\vec{i}m_{dq})}{6V_0} \quad (19)$$

$$\vec{I}_{2_{dq}}^{\Sigma\Delta}=\vec{I}_{2_{dq}c}^{\Sigma\Delta}+\vec{I}_{2_{dq}f}^{\,\Sigma\Delta};\ \vec{I}_{2_{dq}f}^{\,\Sigma\Delta}=\frac{(\vec{v}_{m_{dq}}\vec{i}_{g_{dq}}-\vec{v}_{g_{dq}}\vec{i}_{m_{dq}})}{6V_0} \quad (20)$$

Finally, using (19)−(20) in (17)−(18):

$$Cv_c^*\frac{d\vec{v}_{c_{1dq}}^{\Sigma\Delta}}{dt}\approx-V_0\vec{I}_{1_{dq}c}^{\,\Sigma\Delta*};Cv_c^*\frac{d\vec{v}_{c_{2dq}}^{\Sigma\Delta}}{dt}\approx-V_0\vec{I}_{2_{dq}c}^{\,\Sigma\Delta*} \quad (21)$$

The EFM control is presented in Fig. 2. Using (21), the vector $\vec{v}_{c_{1\alpha\beta}}^{\,\Sigma\Delta}$ is regulated in the dq frame. The dynamic regulation is improved by feed-forwarding the component $\vec{I}_{1dq_f}^{\,\Sigma\Delta}$, which represent the voltage oscillations. The output of the external control loop is multiplied by $f(t)$ and the common-mode voltage is imposed as (16).

3) Control of $\vec{v}_{c_0}^{\,\alpha\beta}$ and $\vec{v}_{c_{\alpha\beta}}^{\,0}$: The dynamics of the vector $\vec{v}_{c_0}^{\,\alpha\beta}$ can be rewritten as:

$$Cv_c^*\frac{d\vec{v}_{c_0}^{\alpha\beta}}{dt}\approx\frac{(\vec{v}_{m_{dq}}\vec{i}_{m_{dq}})e^{-j2\theta_m}}{3\sqrt{2}}-\frac{(\vec{v}_{g_{dq}}\vec{i}_{1dq}^{\,\Sigma\Delta}+\vec{v}_{g_{dq}}\vec{i}_{2dq}^{\,\Sigma\Delta})}{\sqrt{3}} \quad (22)$$

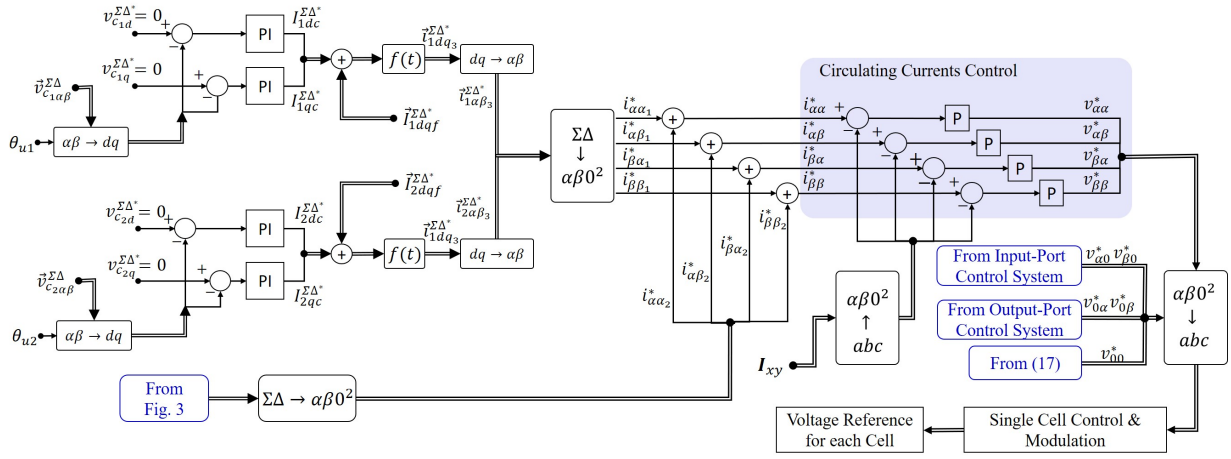

Fig. 2: Proposed Vector Control Strategy for the regulation of the CCVs.

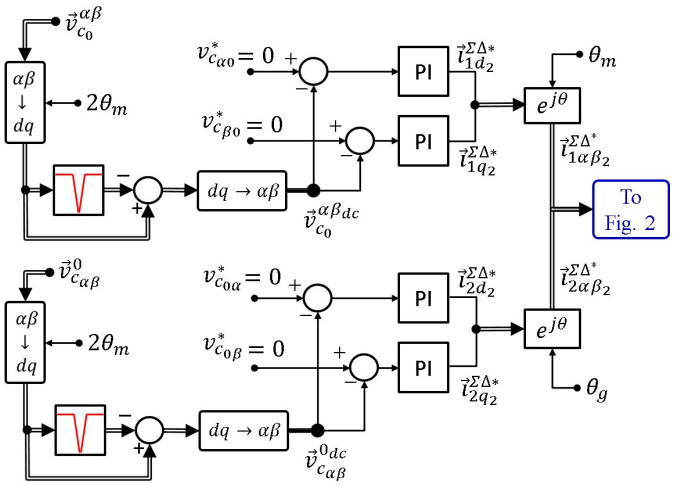

Fig. 3: Proposed LFO Control of $\vec{v}_{c_0}^{\,\alpha\beta}$ and $\vec{v}_{c_{\alpha\beta}}^{\,0}$.

Analogously, $\vec{v}_{c_{\alpha\beta}}^{\,0}$ is expressed as:

$$Cv_c^* \frac{d\vec{v}_{c_{\alpha\beta}}^{0}}{dt} \approx \frac{-(\vec{v}_{g_{dq}} \vec{i}_{g_{dq}}) e^{-j2\theta_g}}{3\sqrt{2}} + \frac{(\vec{v}_{m_{dq}} \vec{i}_{1dq}^{\,\Sigma\Delta} + \vec{v}_{m_{dq}} \vec{i}_{2dq}^{\,\Sigma\Delta})}{\sqrt{3}} \tag{23}$$

Being:

$$\vec{i}_{1\alpha\beta_2}^{\,\Sigma\Delta *} = \vec{i}_{1dq_2}^{\,\Sigma\Delta *} e^{j\theta_g}; \vec{i}_{2\alpha\beta_2}^{\,\Sigma\Delta *} = \vec{i}_{2dq_2}^{\,\Sigma\Delta *} e^{j\theta_m} \tag{24}$$

In EFM, the voltage oscillations in $\vec{v}_{c_0}^{\,\alpha\beta}$ and $\vec{v}_{c_{\alpha\beta}}^{\,0}$ are inside an acceptable range and they can be filtered by the capacitors. Therefore, just the average components of the vectors $\vec{v}_{c_0}^{\,\alpha\beta_{dc}}$, $\vec{v}_{c_{\alpha\beta}}^{\,0_{dc}}$ are regulated using circulating current references in-phase with the input-port and the output-port angles:

$$Cv_c^* \frac{d\vec{v}_{c_0}^{\,\alpha\beta_{dc}}}{dt} \approx -\frac{\vec{v}_{g_{dq}} \vec{i}_{1dq_2}^{\,\Sigma\Delta}}{\sqrt{3}}; Cv_c^* \frac{d\vec{v}_{c_{\alpha\beta}}^{\,0_{dc}}}{dt} \approx -\frac{\vec{v}_{m_{dq}} \vec{i}_{2dq_2}^{\,\Sigma\Delta}}{\sqrt{3}} \tag{25}$$

The proposed Control Strategy is presented in Fig.3. The dc components of the vector $\vec{v}_{c_0}^{\,\alpha\beta}$ are regulated to zero using a power flow in phase with the grid angle θ_g. The same effect is achieved for $\vec{v}_{c_{\alpha\beta}}^{\,0}$ manipulating a non-zero mean active power in phase with the grid angle θ_m.

B. Input and Output Control Systems

Using (1), two independent models are obtained for the input and output port dynamics. The dynamics of the input-output ports Voltage-Current models are controlled using conventional dq control systems implemented in dq coordinates:

$$\begin{bmatrix} v_{md} \\ v_{mq} \end{bmatrix} = \frac{1}{\sqrt{3}} \begin{bmatrix} v_{d0} \\ v_{q0} \end{bmatrix} + \frac{L_c}{3} \frac{d}{dt} \begin{bmatrix} \frac{d}{dt} & -\omega_m \\ \omega_m & \frac{d}{dt} \end{bmatrix} \begin{bmatrix} i_{md} \\ i_{mq} \end{bmatrix} \tag{26}$$

$$-\begin{bmatrix} v_{gd} \\ v_{gq} \end{bmatrix} = \frac{1}{\sqrt{3}} \begin{bmatrix} v_{0d} \\ v_{0q} \end{bmatrix} + \frac{L_c}{3} \frac{d}{dt} \begin{bmatrix} \frac{d}{dt} & -\omega_g \\ \omega_g & \frac{d}{dt} \end{bmatrix} \begin{bmatrix} i_{gd} \\ i_{gq} \end{bmatrix} \tag{27}$$

The voltage references obtained in (26)-(27) are rotated back to Double $\alpha\beta 0$ coordinates resulting in $v_{\alpha 0}$-$v_{\beta 0}$ for the input-port, and $v_{0\alpha}$-$v_{0\beta}$ for the output-port. These references are sent to the Single-Cell Control as shown in Fig. 2.

C. Single-Cell Control and Modulation Scheme

The voltage references obtained by the control systems presented in the previous are transformed to the natural reference frame using the inverse $\alpha\beta 0^2$ Transformation. Then, the Cluster Capacitor Voltage references for each cluster in the abc-rst frame are obtained. Here, an additional control loop is utilised to regulate the capacitor voltages within a cluster at the same level. Readers can refer [6], [13] for more details.

IV. Simulation Results

A 10 MW M^3C has been implemented in PLECS software to validate the theoretical work proposed in this paper. The simulated M^3C has a nominal power of 10 MW and it features seven power cells per cluster. Each power cell capacitor operates at 2 kV with a capacitance of 7 mF. The input-port of the M^3C is connected to an ac system of 5.6 kV, whereas the output port is connected to an ac system of 6.6 kV and 50 Hz.

Results for operation in EFM are presented in Fig. 4 and Fig. 5. The input-port frequency f_m is increased in 2 Hz each 2 seconds until it reaches 50 Hz, as illustrated in Fig. 4(a). The mitigation techniques are applied as proposed in Fig. 2. Accordingly, the oscillations in $\vec{v}_{c_{1\alpha\beta}}^{\,\Sigma\Delta}$ are mitigated using

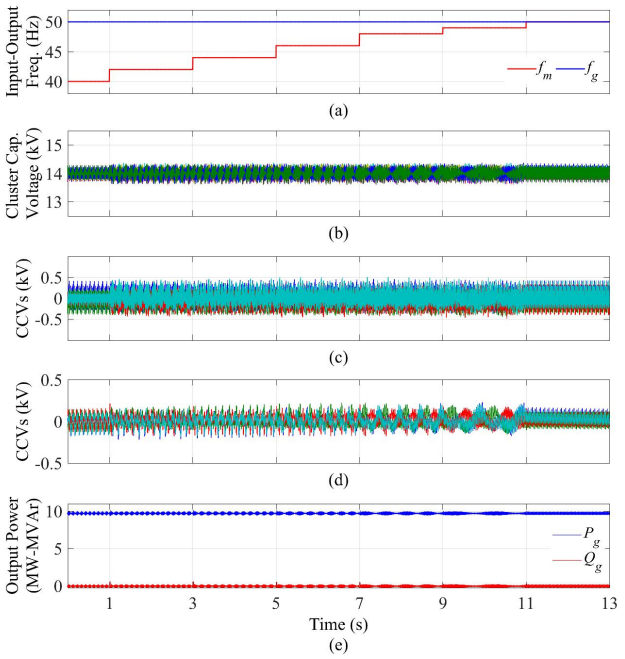

Fig. 4: Simulation Results for EFM. (a) Input and Output ports Frequencies. (b) CCVs. (c) $\vec{v}_{c_0}^{\,\alpha\beta}$ and $\vec{v}_{c_{\alpha\beta}}^{\,0}$. (d) $\vec{v}_{c_{1\alpha\beta}}^{\,\Sigma\Delta}$ and $\vec{v}_{c_{2\alpha\beta}}^{\,\Sigma\Delta}$. (e) Power Injected into the Grid.

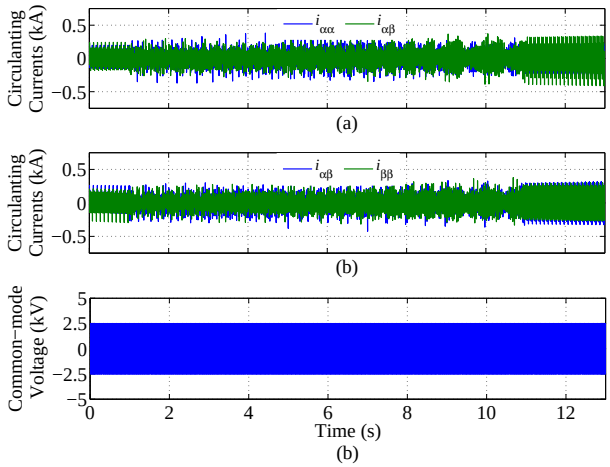

Fig. 5: Simulation Results for EFM. (a) $i_{\alpha\alpha}$ and $i_{\beta\alpha}$. (b) $i_{\alpha\beta}$ and $i_{\beta\beta}$. (c) Common-mode Voltage

the power terms produced by the circulating current and the common-mode voltage.

During all this test, the CCVs are successfully regulated to 14 kV, as shown in Fig. 4(a). The vectors $\vec{v}_{c_0}^{\,\alpha\beta}$ and $\vec{v}_{c_{\alpha\beta}}^{\,0}$ are presented in Fig. 4(b), whereas vectors $\vec{v}_{c_{1\alpha\beta}}^{\,\Sigma\Delta}$ and $\vec{v}_{c_{2\alpha\beta}}^{\,\Sigma\Delta}$ are presented in Fig. 4(c). The four vectors are properly regulated to zero and the voltage oscillations are not increased as f_m gets closer to f_g. Finally, Fig. 4(d) illustrates unity power factor operation of the system injecting 10 MW into the output-port.

Fig. 5(a)−(b) shows the circulating currents for this test. The circulating current peak is bounded at the same amplitude than the pre-equal frequency value ≈ 0.15 kA. This is because the

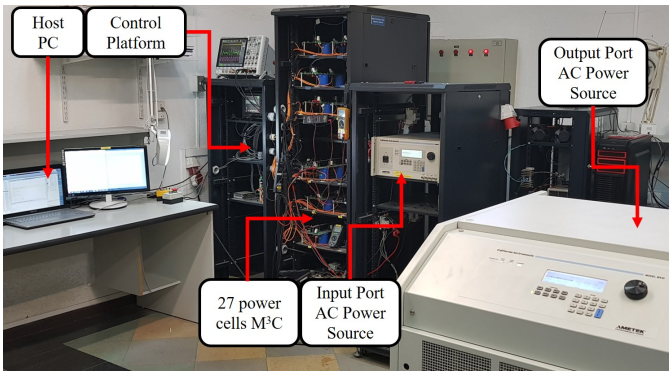

Fig. 6: Downscaled Laboratoy Prototype.

common-mode voltage of Fig. 5(c) is being synthesised to generate manipulable power flows that allow to mitigate the voltage oscillations produced by in EFM. For this test, the common-mode voltage is selected to have an amplitude of 2.5 kV and a fundamental frequency of 120 Hz.

V. Experimental Results

Experimental results for the proposed control methodology have been obtained using the 27-power cell prototype. A photography of it is showed in Fig. 6. The prototype is composed of a control platform and a power stage. The control platform is composed of a Digital Signal Processor (DSP) Texas Instrument board, three FPGA boards, and additional external boards for computer communication and analogue-digital conversion. The power stage of the M^3C prototype is composed of nine clusters based on the series connection of three full-H-bridge cells and one inductor. Therefore, the converter has 27 power cells, each of them connected to a floating capacitor of 4.7mF. The input port has been connected to an Ametek Programmable power source, Model CSW5550. The output-port has been connected to another Ametek Programmable Power Source, Model MX45.

In this test, both port frequencies are set to 50 Hz and the common-mode voltage is defined as (16), considering a peak amplitude of 30 V and 120 Hz (fundamental frequency). Moreover, the input-port is set to operate with $P_m = -3.3$kW and Q_m=0. The output-port is set with P_g=3.3kW and Q_m=2.1KVAr.

As shown in Fig. 7(a), the 27 capacitor voltages are properly controlled to $v_c^* = 150$ V. The vectors $\vec{v}_{c_{1\alpha\beta}}^{\,\Sigma\Delta} - \vec{v}_{c_{2\alpha\beta}}^{\,\Sigma\Delta}$ and $\vec{v}_{c_0}^{\,\alpha\beta} - \vec{v}_{c_{\alpha\beta}}^{\,0}$ are illustrated in Fig. 7(b) and Fig. 7(c), respectively.

In this case, the closed-loop control strategy of Section **??**, ensure that the CCV vectors are effectively regulated to zero. Additionally, the ripple in these vectors is bounded inside a $\pm$ 5 V band, which represents oscillations of $\approx 2.5\%$ of the CCV nominal value.

Oscilloscope waveforms of the voltages and currents of the M^3C are presented. From top to bottom, Fig. **??**(d) shows one of the capacitor voltages of the M^3C $v_{c_{ar1}}$, the cluster voltage v_{ar} and the input-output ports voltages $v_{m_{ab}}$ (purple line) and $v_{g_{rt}}$ (blue line). Finally, Fig. 7(e) shows the grid currents which have a peak amplitude of 14 A.

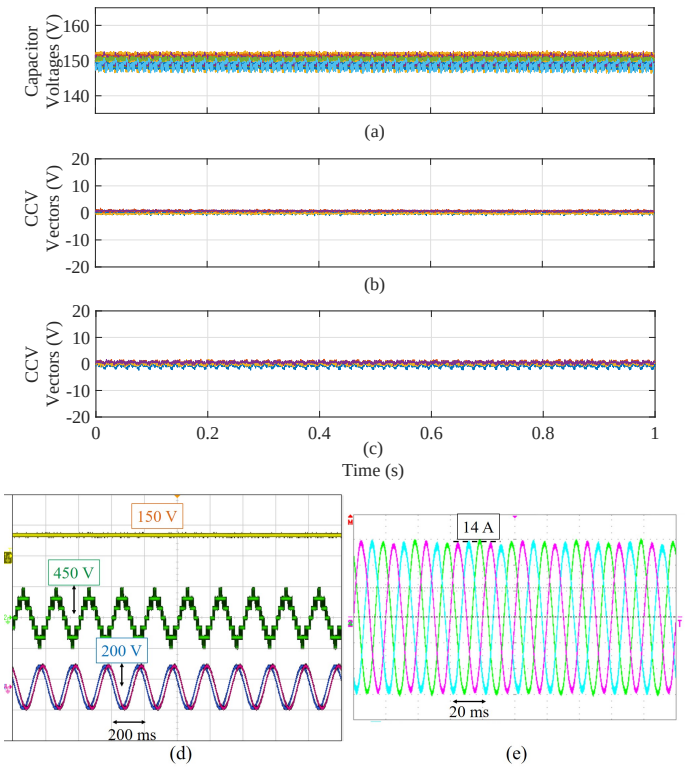

Fig. 7: Experimental Results for EFM. (a) 27 Power Cells Capacitor Voltages. (b) $\vec{v}_{c_0}^{\,\alpha\beta}$ and $\vec{v}_{c_{\alpha\beta}}^{\,0}$. (c) $\vec{v}_{c_{1\alpha\beta}}^{\,\Sigma\Delta}$ and $\vec{v}_{c_{2\alpha\beta}}^{\,\Sigma\Delta}$. (d) Oscilloscope voltage waveforms. (e) Output port currents.

VI. Conclusion

Vector Control Strategies based on the representation of the converter in $\Sigma\Delta$ Double-$\alpha\beta 0$ coordinates has been proposed to enable the operation of the converter in EFM.

In EFM, the Control Strategies consider the use of the circulating currents and common-mode voltage to mitigate the voltage oscillation in the floating capacitor of the converter. It has been proved that the Control System performs closed-loop regulation of the CCV Vectors driving the capacitor voltage oscillations effectively to zero.

The proposed Vector Control Strategies has been analytically discussed and tested through simulations and experiments conducted with a 27 power cell prototype. For all the tests, the regulation of the input and output ports and the control of the oscillations in the floating capacitor voltages have all presented correct performance.

References

[1] R. Erickson, S. Angkititrakul, and K. Almazeedi, "A New Family of Multilevel Matrix Converters for Wind Power Applications: Final Report," University of Colorado, Tech. Rep. December, 2006.

[2] Y. Okazaki, W. Kawamura, M. Hagiwara, H. Akagi, T. Ishida, M. Tsukakoshi, and R. Nakamura, "Which is more suitable for MMCC-based medium-voltage motor drives, a DSCC inverter or a TSBC converter?" in *9th International Conference on Power Electronics - ECCE Asia: "Green World with Power Electronics", ICPE 2015-ECCE Asia*. IEEE, jun 2015, pp. 1053–1060.

[3] F. Kammerer, J. Kolb, and M. Braun, "Fully decoupled current control and energy balancing of the Modular Multilevel Matrix Converter," in *15th International Power Electronics and Motion Control Conference and Exposition, EPE-PEMC 2012 ECCE Europe*. IEEE, sep 2012, pp. LS2a.3–1–LS2a.3–8.

[4] W. Kawamura, M. Hagiwara, and H. Akagi, "Control and experiment of a modular multilevel cascade converter based on triple-star bridge cells," *IEEE Transactions on Industry Applications*, vol. 50, no. 5, pp. 3536–3548, sep 2014.

[5] M. Díaz, R. Cárdenas, B. Mauricio Espinoza, A. Mora, and F. Rojas, "A novel LVRT control strategy for modular multilevel matrix converter based high-power wind energy conversion systems," in *2015 10th International Conference on Ecological Vehicles and Renewable Energies, EVER 2015*. IEEE, mar 2015, pp. 1–11. [Online]. Available:

[6] M. Diaz, R. Cardenas, M. Espinoza, F. Rojas, A. Mora, J. C. Clare, and P. Wheeler, "Control of Wind Energy Conversion Systems Based on the Modular Multilevel Matrix Converter," *IEEE Transactions on Industrial Electronics*, vol. 64, no. 11, pp. 1–1, nov 2017.

[7] B. Fan, K. Wang, P. Wheeler, C. Gu, and Y. Li, "A Branch Current Reallocation Based Energy Balancing Strategy for the Modular Multilevel Matrix Converter Operating Around Equal Frequency," *IEEE Transactions on Power Electronics*, vol. 33, no. 2, pp. 1105–1117, feb 2018.

[8] M. Diaz, R. Cárdenas, M. Espinoza, A. Mora, and P. Wheeler, "Modelling and control of the Modular Multilevel Matrix Converter and its application to Wind Energy Conversion Systems," in *IECON 2016 - 42nd Annual Conference of the IEEE Industrial Electronics Society*, no. 1140337. IEEE, oct 2016, pp. 5052–5057. [Online]. Available:

[9] W. Kawamura, Y. Chiba, M. Hagiwara, and H. Akagi, "Experimental Verification of an Electrical Drive Fed by a Modular Multilevel TSBC Converter When the Motor Frequency Gets Closer or Equal to the Supply Frequency," *IEEE Transactions on Industry Applications*, vol. 53, no. 3, pp. 1–1, may 2017.

[10] M. Espinoza, R. Cárdenas, M. Díaz, A. Mora, and D. Soto, "Modelling and control of the modular multilevel converter in back to back configuration for high power induction machine drives," in *IECON Proceedings (Industrial Electronics Conference)*. IEEE, oct 2016, pp. 5046–5051.

[11] F. Kammerer, M. Gommeringer, J. Kolb, and M. Braun, "Energy balancing of the Modular Multilevel Matrix Converter based on a new transformed arm power analysis," in *2014 16th European Conference on Power Electronics and Applications, EPE-ECCE Europe 2014*. IEEE, aug 2014, pp. 1–10.

[12] M. Espinoza, E. Espina, M. Diaz, A. Mora, and R. Cardenas, "Improved control strategy of the modular multilevel converter for high power drive applications in low frequency operation," in *2016 18th European Conference on Power Electronics and Applications (EPE'16 ECCE Europe)*. IEEE, sep 2016, pp. 1–10. [Online]. Available:

[13] H. Akagi, S. Inoue, and T. Yoshii, "Control and Performance of a Transformerless Cascade PWM STATCOM With Star Configuration," *IEEE Transactions on Industry Applications*, vol. 43, no. 4, pp. 1041–1049, 2007.